Separation and Purification Technology 206 (2018) 226–238

Contents lists available at ScienceDirect

Separation and Purification Technology

journal homepage: www.elsevier.com/locate/seppur

Silver vanadium oxide materials: Controlled synthesis by hydrothermal method and efficient photocatalytic degradation of atrazine and CV dye

Chiing-Chang Chen[a], Janah Shaya[b], Huan-Jung Fan[c], Yi-Kuo Chang[d], Han-Ting Chi[a], Chung-Shin Lu[e,*]

[a] Department of Science Education and Application, National Taichung University of Education, Taichung 403, Taiwan, ROC
[b] Institut de Physique et Chimie des Matériaux (IPCMS), UMR 7504, CNRS-Université de Strasbourg, 23 Rue du Loess, 67034 Strasbourg Cedex 2, France
[c] Department of Environmental Engineering, HungKuang University, Sha-Lu, Taichung 433, Taiwan, ROC
[d] Department of Safety Health and Environmental Engineering, Central Taiwan University of Science and Technology, Taichung 406, Taiwan, ROC
[e] Department of General Education, National Taichung University of Science and Technology, Taichung 404, Taiwan, ROC

ARTICLE INFO

Keywords:
Photocatalysis
Silver vanadate
Visible light
Atrazine
Crystal violet
Water treatment

ABSTRACT

Silver vanadium oxides have received remarkable attention in recent years because of their stability, suitable band gaps, and relatively superior photocatalytic abilities. This study reports the synthesis of silver vanadates by the hydrothermal method and the investigation of their photocatalytic abilities for removing crystal violet (CV) and atrazine pollutants under visible-light irradiation. The as-prepared silver vanadates are characterized by X-ray diffraction (XRD), scanning electron microscopy (SEM), X-ray photoelectron spectroscopy (XPS), and UV–vis diffuse reflectance spectra (DRS). Crystal violet and atrazine could be successfully degraded in the presence of the silver vanadate catalyst under visible-light irradiation. The obtained results show complete degradation of crystal violet after 24 h of treatment and over 97% degradation of atrazine after 72 h. The as-prepared silver vanadate materials show extremely high catalytic stability and maintain stable activity after three catalytic cycles. The scavenger studies indicate that $^{\cdot}O_2^-$ radicals are the main active species in the degradations of CV and atrazine, while $^{\cdot}OH$ and h^+ play an assistant role in these processes. Liquid chromatography coupled with electrospray ionization mass spectrometry is used to analyze the samples obtained from the photocatalytic degradation of CV and atrazine. The degradation pathways of atrazine are evaluated suggesting two different routes including dechlorination–hydroxylation and alkylic-oxidation–de-alkylation. On the other hand, the degradation of the CV takes place via *N*-de-methylation in a stepwise manner generating the various *N*-de-methylated intermediate CV species. The excellent activity and photostability reveal that silver vanadates (including $Ag_4V_2O_7$) are promising visible-light-responsive photocatalysts for water and wastewater treatment.

1. Introduction

Semiconductor photocatalysts have attracted strong attention due to their efficiency in environmental purifications and splitting of water into hydrogen and oxygen gases [1–4] in addition to the importance of catalysis in various domains of research. Silver-based oxides, with the unique hybridized valence bands (O 2p and Ag 4d orbitals), exhibit a narrow band gap (≤3 eV) and highly dispersed valence bands (VB), resulting in useful photoabsorption ability and high mobility of photoholes, respectively. Therefore, these materials are prospective candidates as visible-light-sensitive photocatalysts in interesting applications [5–7]. Among the different silver-based semiconductors, the efficiency of silver vanadium oxide materials (silver vanadates, SVO) in photocatalytic applications using visible irradiation has been documented, owing to their narrow band gap and good crystallization [8–11]. SVO materials are among the most complex metal oxides, with a number of phases present even in the case of a single atomic composition [12,13]. Moreover, SVO semiconductors exhibit a band gap transition that allows strong absorption in the visible light region [14]. They also have potential uses in rechargeable high-energy density lithium batteries, solar energy conversions, and sensors [15–18].

Significant effort has been devoted in the past years to synthesize different types of silver vanadates as well as different morphologies [19–21]. Nevertheless, there are few studies that describe the impact of the preparation factors on these vanadates such as the ratio of the silver and vanadium sources, which has not yet been probed, and the effect of the pH on the preparation [22]. Specifically, there exist four main types of silver vanadates: $AgVO_3$, $Ag_2V_4O_{11}$, Ag_3VO_4, and $Ag_4V_2O_7$. Among

* Corresponding author at: 129, Sec. 3, San-min Rd., Taichung, Taiwan 40401, Taiwan, ROC.
E-mail address: cslu6@nutc.edu.tw (C.-S. Lu).

https://doi.org/10.1016/j.seppur.2018.06.011
Received 3 February 2018; Received in revised form 18 May 2018; Accepted 3 June 2018
Available online 04 June 2018
1383-5866/

Table 1
Catalyst codes and crystalline phases of the silver vanadate samples prepared under different reaction conditions.

Catalyst code	Molar ratio	pH	Crystalline phase
Ag1V1-5	1:1	5	$AgVO_3$
Ag1V1-7	1:1	7	$AgVO_3$
Ag1V1-9	1:1	9	$AgVO_3$
Ag2V1-5	2:1	5	$Ag_4V_2O_7$
Ag2V1-7	2:1	7	$Ag_4V_2O_7$
Ag2V1-9	2:1	9	$Ag_4V_2O_7$
Ag3V1-5	3:1	5	$Ag_4V_2O_7$
Ag3V1-7	3:1	7	$Ag_4V_2O_7 + Ag_3VO_4$
Ag3V1-9	3:1	9	$Ag_4V_2O_7 + Ag_3VO_4$

them, Ag_3VO_4 shows the highest photocatalytic activity. Research has generally overlooked the activity of $Ag_4V_2O_7$, which often coexists with Ag_3VO_4, and investigations that focus on the photocatalytic efficiency of $Ag_4V_2O_7$ are *hitherto* limited [11,14,23]. Wang et al. have shown that pure $Ag_4V_2O_7$ materials prepared by the hydrothermal method exhibit high photocurrent response, strong absorption in the region of visible light, and high catalytic efficiency in RhB photodegradation using visible irradiation [22]. Hence, $Ag_4V_2O_7$ has potential applications as visible-light-sensitive photocatalysts in the removal and decomposition of organic pollutants. In the continuity of our research related to photocatalysis and degradation of contaminants [24–28], we have been interested in the preparation of $Ag_4V_2O_7$ and its applications in the photocatalytic decomposition of toxic molecules under visible-light irradiation.

Considering organic contaminants, atrazine herbicides are widely used to control grassy weeds in cotton, corn, soybean, rice, and wheat crop fields. Currently, around forty types of common herbicides contain atrazine as one of the basic ingredients, and more than sixty countries utilize this organic compound [29]. Atrazine and its byproducts are known to be mutagens, possible carcinogens, and endocrine disruptors that persist in the environment, making their way into both surface and ground water [30,31]. These compounds have been frequently detected in water supplies causing serious pollution problems, especially due to their long half-lives. According to USEPA, long exposure to atrazine has led to mammary gland tumors and endocrine perturbations in studies carried out on animals. Moreover, even low quantities of atrazine can adversely influence the sexual development of amphibians [32]. Hence, the negative impact of atrazine and similar pollutants on ecosystems and human health urges further investigations in order to develop efficient and environmentally friendly technologies for water treatment.

On the other hand, dyes constitute a widely used class of chemicals for industrial and medicinal uses [33–38]. A great variety of dyes are classified as environmental pollutants, which have different effects ranging from skin irritations and moderate toxicity to more serious carcinogenic and mutagenic effects on the aquatic system. The process of detection of dyes is complex due to the diversity of functional groups in different dyes. Crystal violet [Tris((dimethylamino)phenyl) methylium chloride] dye is very stable and non-biodegradable due to the electron-donating group in its unique structure. It is a known carcinogen, which raises concern as most of the commonly used primary and secondary aromatic amines [39,40]. Thus, various semiconductors are being studied in the removal of dyes [41–43].

The traditional techniques of water treatment involve biological treatments, chemical oxidations, and activated carbon adsorptions, among others. These methods suffer from limitations. For instance, biological treatments need the disposal of activated sludge and are still long processes due to the slow rates of these reactions. The adsorption

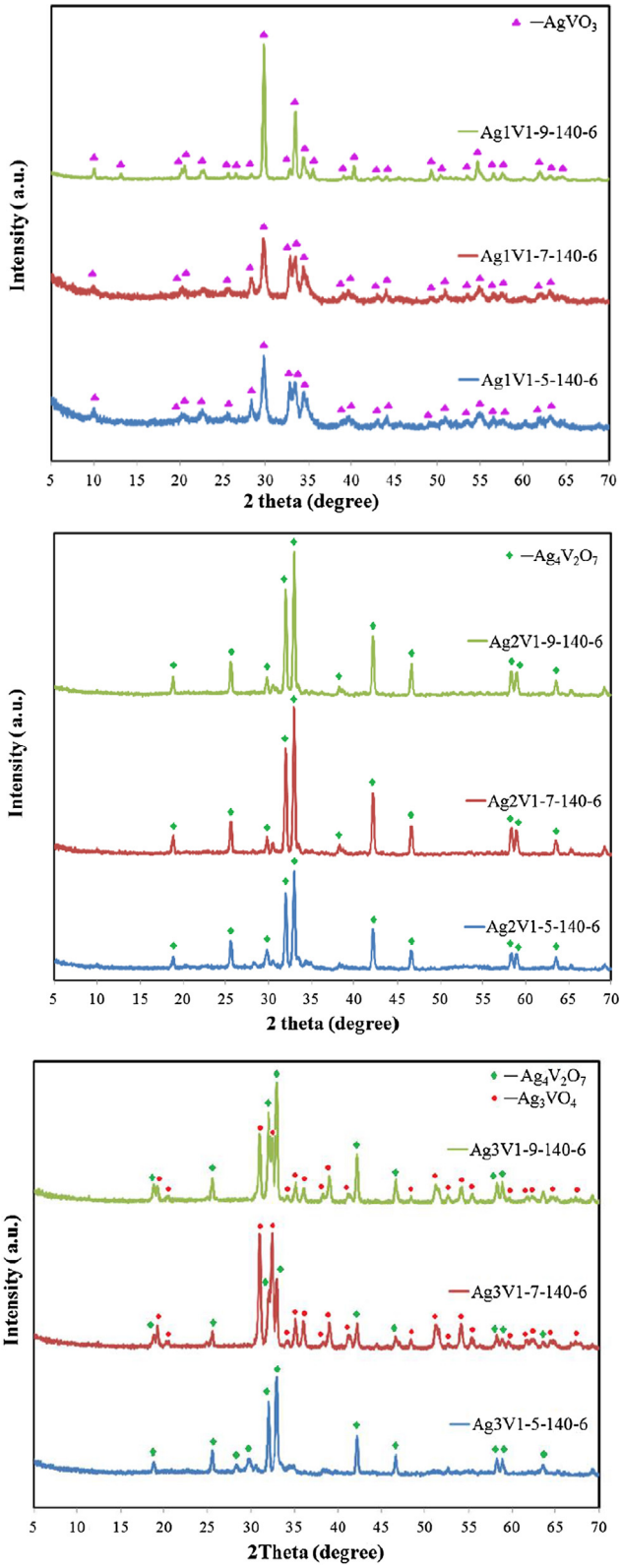

Fig. 1. XRD patterns of the as-prepared silver vanadate samples under different pH values and Ag/V molar ratio, at reaction temperature 140 °C and reaction time 6 h.

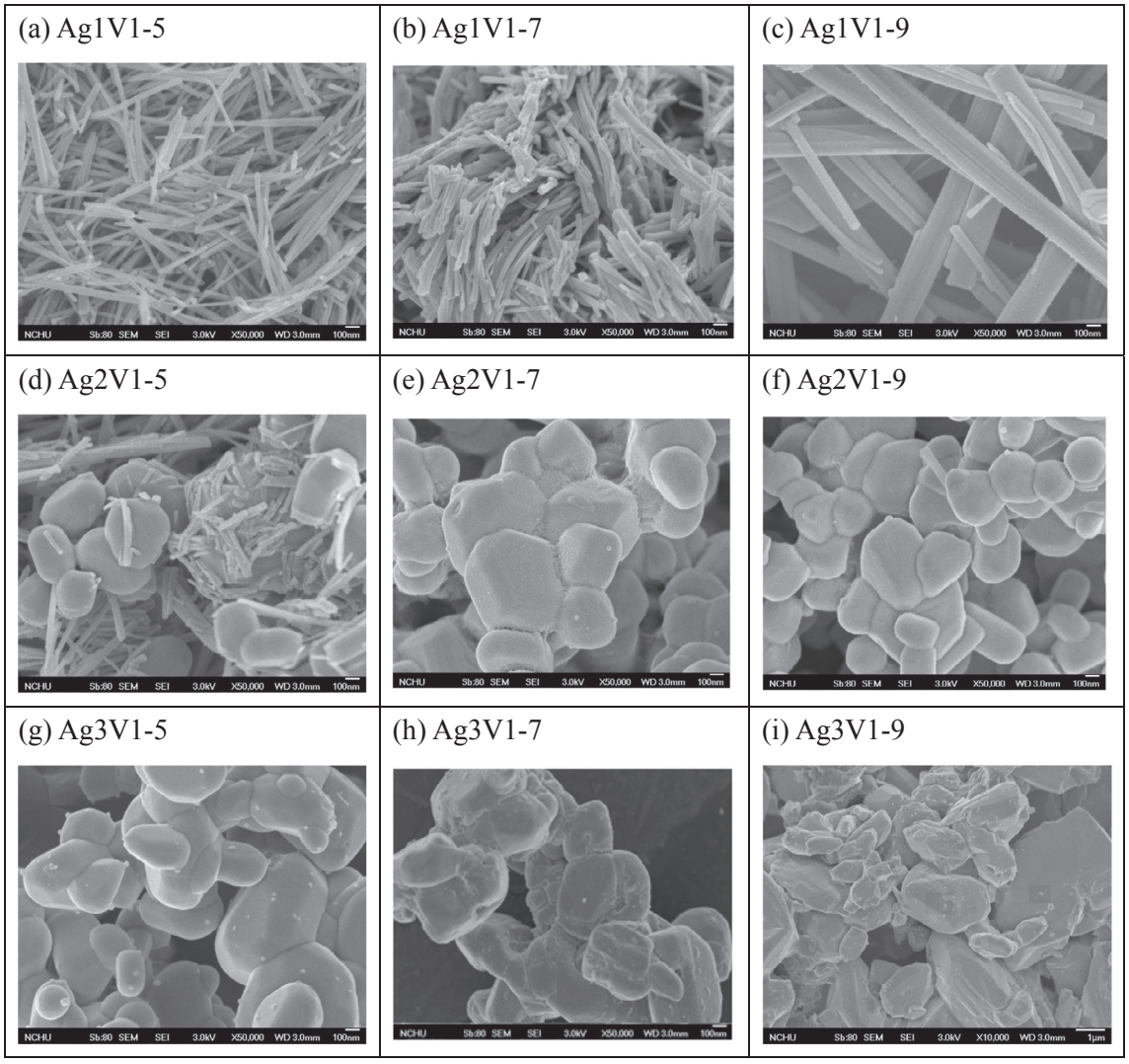

Fig. 2. SEM images of the silver vanadate samples prepared by the hydrothermal autoclave method at different pH values and Ag/V molar ratio.

methods do not include the degradation of the products but their phase transfer only [25]. In contrast, the semiconductors ensure the catalytic photodegradation of a wide range of pollutants into less harmful or completely non-toxic products under ambient conditions and without the use of additives. Therefore, photocatalysis is emerging as one of the most effective tools of wastewater treatment [24,25,44–46].

The current work presents the synthesis of various silver vanadates by the hydrothermal process including $Ag_4V_2O_7$ material. The impact of the factors of hydrothermal preparation including the ratio of starting materials and the pH value on the structure-properties of silver vanadates is elaborated. Next, the photocatalytic activity of the obtained semiconductors is examined in the degradation of atrazine and CV at different conditions under visible-light irradiation. Moreover, the influence of scavengers of active species on the photocatalytic activity is probed in detail and the stability of the photocatalyst is tested for three successive runs. Finally, the intermediates of the photocatalytic degradation are identified by LC/MS, and the possible degradation pathways of CV and atrazine by silver vanadates are proposed.

2. Experimental

2.1. Materials

The purchased atrazine from Sigma-Aldrich and CV dye from Tokyo Kasei Kogyo Co. were used without any further purification. A stock solution containing 10 mg L^{-1} of atrazine (or CV) in water was prepared, protected from light, and stored at 4 °C. HPLC analysis was used to confirm the presence of atrazine (or CV dye) as a pure organic compound. Silver nitrate $AgNO_3$ (Aldrich, 99%) and ammonium metavanadate NH_4VO_3 (Panreac, 99%) were used as the sources of the silver and vanadates in the photocatalysts, respectively. Reagent-grade ammonium acetate, sodium hydroxide, nitric acid, and HPLC-grade methanol were purchased from Merck. Deionized water was used throughout this study. The water was purified with a Milli-Q water ion-exchange system (Millipore Co.) for a resistivity of 1.8×10^7 Ω-cm.

2.2. Preparation and characterization of silver vanadates

In a typical procedure, NH_4VO_3 powder was put into a beaker with 20 mL hot de-ionized water (80 °C) to form a transparent solution, which was then cooled to room temperature. Subsequently, the aqueous $AgNO_3$ solution was added drop-wise to the NH_4VO_3 solution under vigorous stirring for 0.5 h. The ratio of silver to vanadium in the starting materials was kept in a stoichiometric ratio (Ag: V = 1:1, 2:1, 3:1). The final pH value of the solution was adjusted to 5–9 using ammonia solution, followed by additional stirring at room temperature for 12 h. The obtained slurry was then transferred into a Teflon-lined stainless steel autoclave and heated to 140 °C for 6 h. After being naturally

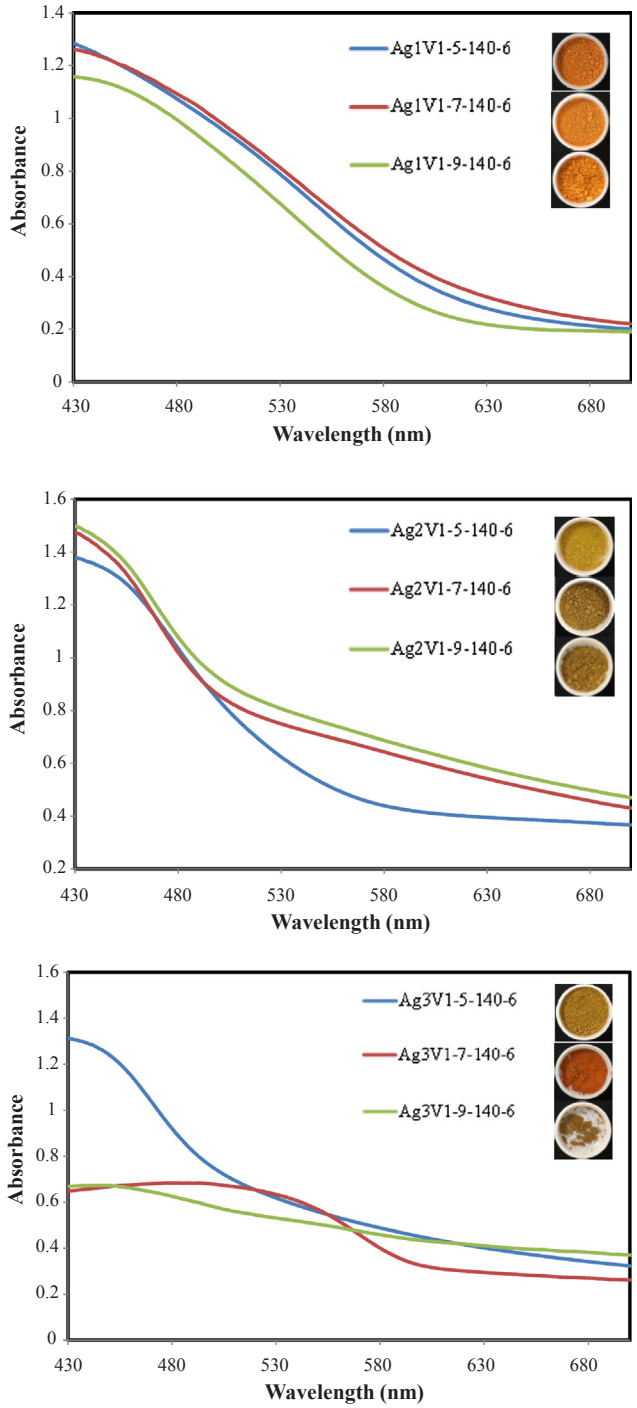

Fig. 3. UV–vis absorption spectra of the prepared silver vanadate samples under different pH values and Ag/V molar ratio. The inset shows the color of the obtained silver vanadate samples.

cooled to room temperature, the obtained precipitate was collected by filtration, washed several times with absolute ethanol and distilled water, and dried at 60 °C for 12 h. Depending on the $AgNO_3/NH_4VO_3$ molar ratio (Ag : V = 1:1, 2:1, 3:1) and the pH value (5, 7, 9), the silver vanadate samples were prepared and marked as shown in Table 1; the as-prepared samples were labeled using Ag1V1-5 through Ag3V1-9.

The phase and composition of the as-prepared silver vanadates were measured using an X-ray diffractometer (PHILIPS X'PERT Pro MPD). The morphology of the silver vanadates was analyzed using a field-emission scanning electron microscope (FE-SEM, HITACHI S-4800). The UV–vis diffuse reflectance spectra of the silver vanadates were measured using a UV–vis spectrophotometer equipped with an integration sphere (Perkin Elmer Lambda 35). The binding energy of Ag, V, and O was measured at room temperature using an X-ray photoelectron spectroscope (XPS, VG Scientific ESCALAB 250). The peak position of each element was corrected by C1s (284.6 eV). The Brunauer-Emmett-Teller (BET) surface area of the silver vanadates was analyzed by nitrogen adsorption-desorption measurement (ASAP 2020).

2.3. Apparatus and instruments

The apparatus used to study the photocatalytic degradation of the CV and atrazine is described elsewhere [47]. The C-75 Chromato-Vue UVP cabinet provided a wide area of illumination from 4 W visible-light tubes positioned on two sides of the cabinet interior. A Waters ZQ LC/MS system, equipped with a binary pump, a photodiode array detector, an autosampler, and a micromass detector, was used for separation and identification.

2.4. Procedures and analyses

The aqueous suspensions of atrazine (or CV) (100 mL, 10 mg L^{-1}) and the photocatalyst powder (0.1 g) were mixed and used in the photocatalytic experiments. For reactions in different pH media, the initial pH of the suspension was adjusted by adding either NaOH or HNO_3 solution. Prior to irradiation, the suspension was magnetically stirred in the dark for ca. 30 min to ensure the establishment of adsorption/desorption equilibrium. Irradiation was carried out using two fluorescent lamps (F4T5/CW, Philips Lighting Co.). The lamp mainly provides visible light in the range of 400–700 nm. The average light intensity striking the surface of the reaction solution was about 1420 lx, as measured by a digital luxmeter. At any given irradiation time interval, the suspension was sampled (5 mL) and centrifuged to separate the silver vanadate powders.

After each irradiation cycle, the amount of the atrazine (or CV) residue was determined by HPLC. The analysis of organic intermediates was accomplished by HPLC-ESI-MS after readjusting the chromatographic conditions to make the mobile phase compatible with the working conditions of the mass spectrometer. Solvent A was 25 mM aqueous ammonium acetate buffer (pH 6.9), and solvent B was methanol. LC was carried out on an Atlantis™ dC_{18} column (250 mm × 4.6 mm i.d., dp = 5 μm). The flow rate of the mobile phase was set at 1 mL/min. A linear gradient was run as follows: t = 0, A = 95, B = 5; t = 20, A = 50, B = 50; t = 35–40, A = 10, B = 90; and, t = 45, A = 95, B = 5. The elution was monitored at 220 nm for atrazine or 580 nm for CV runs. The column effluent was introduced into the ESI source of the mass spectrometer. The quadruple mass spectrometer, equipped with an ESI interface with a heated nebulizer probe at 350 °C, was used with an ion source temperature of 80 °C. ESI was carried out with the vaporizer at 350 °C, and nitrogen was used as sheath (80 psi) and auxiliary (20 psi) gas to assist with the preliminary nebulization and to initiate the ionization process. A discharge current of 5 μA was applied. The tube lens and capillary voltages were optimized for maximum response during the perfusion of the atrazine (or CV) standard.

Table 2
Composition and characterization of silver vanadates.

Catalyst code	EDS element atomic ratio (%)			Energy gap (eV)	BET (m^2/g)
	Ag	V	O		
Ag1V1-5	12.46	11.00	76.53	1.90	24.55
Ag1V1-7	13.96	12.98	73.06	1.85	29.40
Ag1V1-9	19.76	17.08	63.16	1.96	32.38
Ag2V1-5	21.37	11.62	67.00	2.15	9.78
Ag2V1-7	22.23	11.42	66.35	2.25	2.04
Ag2V1-9	21.05	8.75	70.20	2.23	1.84
Ag3V1-5	25.72	12.87	61.41	2.21	3.96
Ag3V1-7	33.43	11.34	55.22	1.90	0.99
Ag3V1-9	31.69	13.30	55.01	–	0.22

3. Results and discussion

3.1. Characterization of the as-prepared powders

The X-ray diffraction patterns of the obtained silver vanadate photocatalysts with various hydrothermal parameters are depicted in Fig. 1. To simplify the discussion, the codes and the crystalline phases of the prepared samples under different ratios and pH values are illustrated in Table 1. Three types of XRD patterns can be distinguished for the prepared samples by hydrothermal synthesis. The different characteristic peaks are assigned to the pure β-$AgVO_3$ (JCPDS 29-1154), pure $Ag_4V_2O_7$ (JCPDS 77-0097), and to the mixed phases of $Ag_4V_2O_7$ and α-Ag_3VO_4 (JCPDS 43-0542), respectively [1]. When the ratio of silver to vanadium was 1.0, the diffraction peaks can be readily indexed to the pure phase of β-$AgVO_3$ monoclinic structure. When the Ag/V ratio was 2.0, the diffraction peaks can be attributed to the pure phase of $Ag_4V_2O_7$ orthorhombic structure. The pH had no effect on the composition or on the structure of the prepared silver vanadates at Ag/V ratio = 1.0 or 2.0; slight lowering and widening of the XRD diffraction peaks were only observed as the pH decreased. On the other hand, the influence of pH value was more noticeable in the hydrothermal synthesis of the silver vanadates when the Ag/V ratio became 3.0. At pH = 7, 9 and Ag/V ratio = 3.0, the diffraction peaks showed two sets of diffraction lines: the first set can be assigned to the α-Ag_3VO_4 structure, while the second set can be ascribed to $Ag_4V_2O_7$. Accordingly, the Ag3V1-7 and Ag3V1-9 samples had mixed phases of $Ag_4V_2O_7$ and α-Ag_3VO_4 [48]. However, at pH = 5 and Ag/V ratio = 3.0, all the peaks corresponding to α-Ag_3VO_4 disappeared, and pure $Ag_4V_2O_7$ was obtained. It can be concluded that the molar ratio of silver to vanadium has a principal role in these experiments, whereas the pH plays a minor role in controlling the composition of the semiconductor products.

The influences of the Ag/V molar ratios and pH values on the morphologies of the silver vanadate samples were investigated. Fig. 2 displays the SEM images of the as-prepared silver vanadates at various conditions. As can be seen in Fig. 2(a–i), the shape of the silver vanadate particles with Ag/V ratio = 1.0 was rod-like with a width of 0.05–0.1 μm and a length of several micrometers. In addition, the pH value had little effect on the morphology of the synthesized silver vanadates since the different pH values did not impose a significant change in the prepared samples with the same Ag/V molar ratio [Fig. 2(a–c)]. However, the SEM images showed that the morphology of the silver vanadates obtained at a higher Ag/V molar ratio changed from rod-like particles to irregular particles. The samples synthesized at molar ratios 2.0 and 3.0 showed particles of irregular shape with a smooth surface and a varying particle size between 0.1 and 0.5 μm [Fig. 2(e–i)]. These results are in line with the XRD data, signifying the important impact of the Ag/V molar ratio and the minor effect of the pH value during the synthesis.

The main factor that determines the photocatalytic activity of a semiconductor is its optical absorption property, which is related to its electronic structure [49]. Fig. 3 shows the UV–vis diffuse reflectance

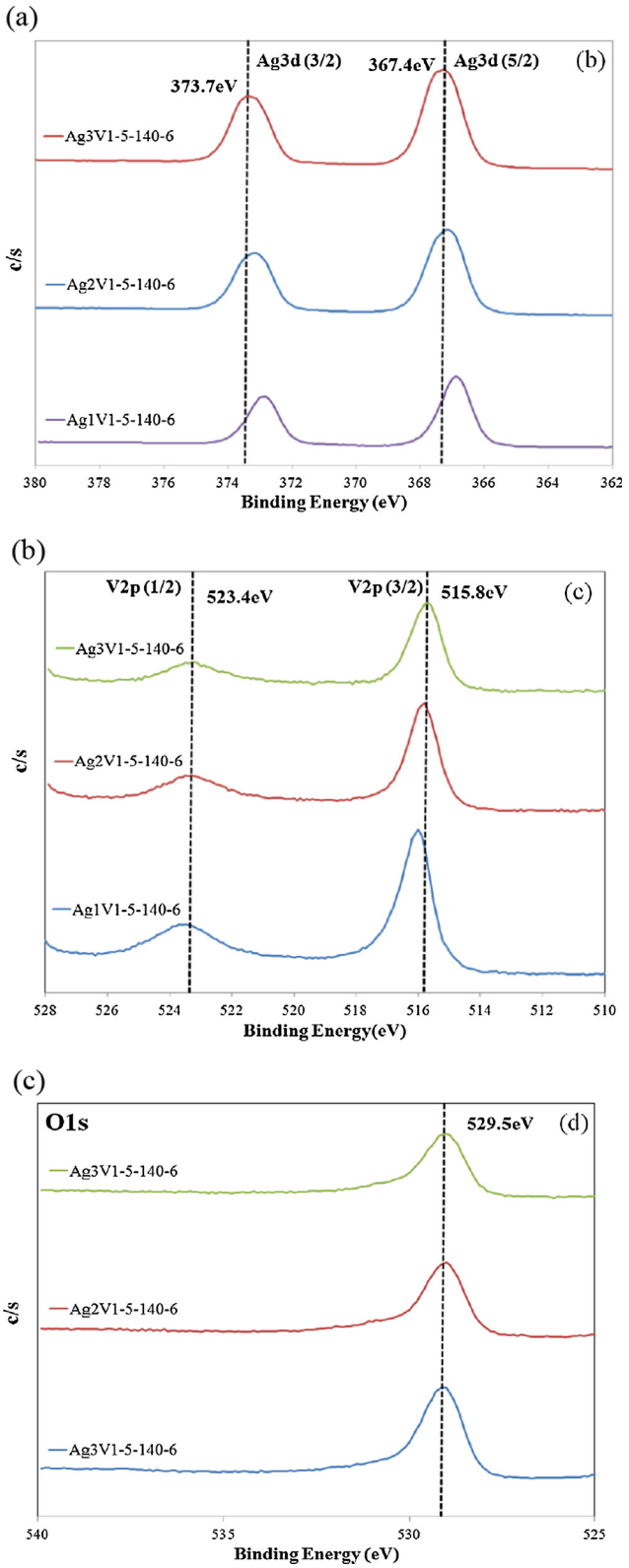

Fig. 4. High-resolution XPS spectra of silver vanadate prepared by the hydrothermal autoclave method under different Ag/V molar ratio, pH = 5. (a) Ag 3d; (b) V 2p; (c) O 1s.

spectra of the as-prepared silver vanadate samples. All the samples absorbed strongly in the visible light range. This eminent absorption favors the use of the photocatalytic activity of these samples under visible-light irradiation. The estimation of the band gaps of the silver

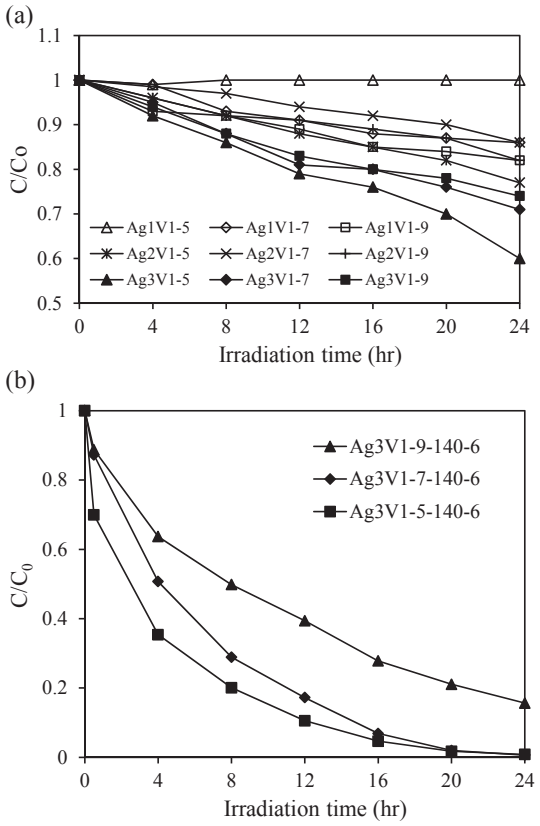

Fig. 5. Photocatalytic degradation of atrazine and CV by the resulting silver vanadate catalysts under visible light irradiation. (a) Atrazine; (b) CV.

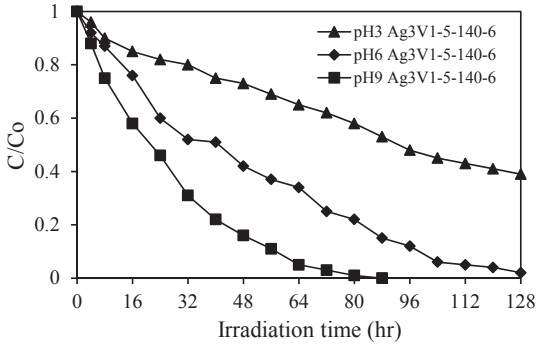

Fig. 6. pH effect on the photocatalytic degradation rate of atrazine. Experimental conditions: atrazine concentration 10 mg L^{-1}; catalyst concentration 1.0 g L^{-1}.

vanadates was achieved using the following equation: $ah\nu = A(h\nu - Eg)^{n/2}$ [50]. The estimated values are depicted in Table 2 and were found to be 1.85–2.25 eV from the onset of the absorption edges. Some factors such as the size of the coupled oxides, the changes of the crystalline phases, the individual compositions of the samples, in addition to the defects might account for the differences in the band gap energy [49,51].

The color of the synthesized samples offers further hints of their different components and structures. The inset in Fig. 3 reveals that Ag1V1-5 sample is orange in color, Ag2V1-5 sample is chrome yellow, and Ag3V1-5 sample is dark goldenrod. Thus, it can be noticed that the color of the silver vanadates became darker with the increase in the Ag/V ratio. The color of the obtained catalysts was also dependent on the pH value and changed from dark goldenrod (Ag3V1-5) to reddish brown (Ag3V1-7). Fig. 3b and c show the extra absorption (530–630 nm) for the catalysts obtained at pH = 7, 9 compared to the catalysts obtained at pH = 5. Accordingly, the color of the catalysts obtained at pH = 7, 9 is much darker than the catalysts obtained at pH = 5. The absorption spectra are consistent with the colors of the powders. However, the clear sharp cut off was not observed for Ag3V1-7 and Ag3V1-9 samples, and this indicates the slight impurity present in these materials. The EDS and the BET specific surface areas of the samples are also shown in Table 2 and in the supplementary data (Fig. 1S and 2S). The EDS shows the main elements of these samples (Ag, V, and O). The Ag/V atomic ratios of the silver vanadate samples were within the range of 1.08–2.95, which correspond to $AgVO_3$, $Ag_4V_2O_7$, and $Ag_4V_2O_7/Ag_3VO_4$ phases. The BET data will be discussed in the section related to the photocatalytic activity (*vide infra*).

As a final characterization step, XPS analyses were conducted to confirm the chemical and electronic states present in the different photocatalysts. The XPS spectra of the obtained silver vanadates are disclosed in Fig. 4(a–c), showing the characteristic spin-orbit split signals of Ag $3d_{3/2}$ and Ag $3d_{5/2}$ signals as well as the signals of V $2p_{1/2}$ and V $2p_{3/2}$ and the O 1s peak. The spectra of the Ag species (Fig. 4a) manifested two symmetric peaks located at 367.4 and 373.7 eV binding energies with a separation of 6 eV. These peaks are attributed to the spin-orbit splitting characteristic of Ag $3d_{5/2}$ and Ag $3d_{3/2}$, respectively; which conform to Ag^+ ion. Fig. 4b exhibited a peak at 515.8 eV binding energy, which is ascribed to V $2p_{3/2}$ orbital, in addition to another peak at 523.4 eV that corresponds to the V $2p_{1/2}$ orbital. These peaks signify that V^{5+} is the form of the vanadium species present in the prepared silver vanadates. Lastly, the obtained O 1s peak in Fig. 4c at 529.5 eV is attributed to the lattice oxygen in the crystalline silver vanadate [25,52].

3.2. Photocatalytic reactions

The photocatalytic activity of the silver vanadates was evaluated by examining the degradation of atrazine and CV dye in water under visible light irradiation. Fig. 5(a and b) portrays the profile of the photodegradation efficiency of these two molecules versus time. The degradation of both atrazine and CV could not take place under visible light irradiation in the absence of the photocatalysts. The presence of the silver vanadates significantly improved the removal efficiencies of these substances. The prepared catalysts were more efficient in the photodegradation of CV. It can be seen from the figure that the degradation of the CV dye is faster than the degradation of the organic contaminant (atrazine) in the case of Ag3V1 samples. The complete degradation of the CV dye took place within 24 h, while 40% of atrazine degradation was achieved in 24 h of irradiation with visible light. These results clearly indicate that the photocatalytic activity of $Ag_4V_2O_7$ (Ag3V1-5) is higher than the other silver vanadate samples including the one with pure $AgVO_3$, and they also reveal that this activity varies with the nature of the substances. Hwang et al. have indicated that an efficient photocatalyst requires a high surface area and a high crystallinity because many reaction steps of photocatalysis take place on the surface and a defect in the structure can provide a site for the electron-hole recombination [53]. In Table 2, it can be seen that the surface area of Ag1V1 samples was estimated to be 24.55–32.38 $m^2 g^{-1}$, which was larger than the area of Ag2V1 samples (1.84–9.78 $m^2 g^{-1}$) and Ag3V1 samples (0.22–3.96 $m^2 g^{-1}$). However, the photocatalytic degradation of atrazine showed the following trend (Fig. 5): Ag3V1 > Ag2V1 > Ag1V1. The present results indicate that the specific surface area of

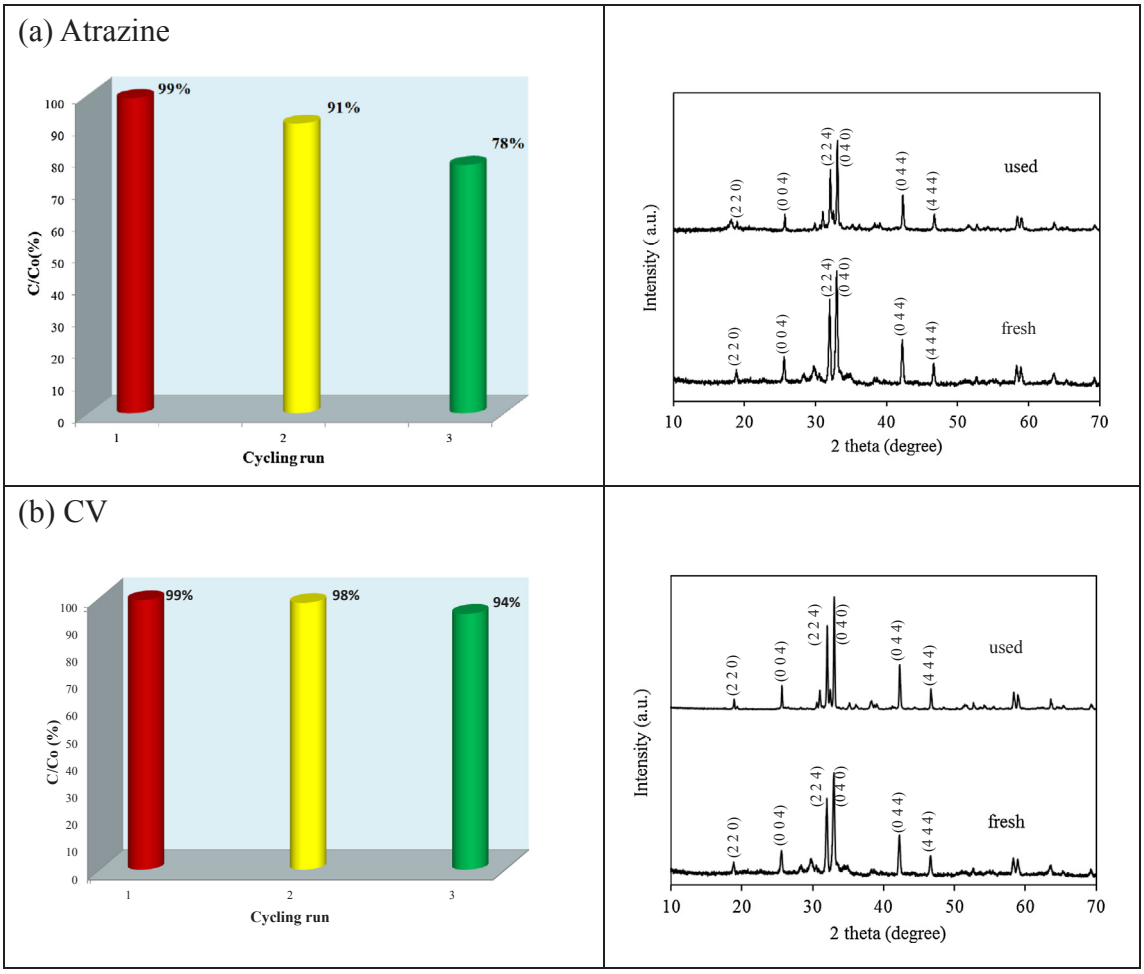

Fig. 7. Cycling runs and XRD patterns acquired before and after the photocatalytic degradation of (a) atrazine and (b) CV in the presence of silver vanadate catalyst.

SVO is not the major factor that controls the photocatalytic activity. The crystallinity and crystalline phase appear to be more important than the surface area in the atrazine degradation.

The impact of the initial pH of solution on the photodegradation of organic compounds has been reported in the literature [42,46,54]. This important parameter was investigated and the effects of the initial pH on the photodegradation rate of atrazine for the $Ag_4V_2O_7$ suspensions are shown in Fig. 6. The results indicated that the decrease in pH led to a decrease in the rate of degradation, while an alkaline medium (increase in pH) resulted in a faster reaction. Specifically, raising the initial pH from 3.0 to 9.0, the degradation rate of atrazine significantly increased from 42% to 99% within 80 h. The faster photodegradation rate in alkaline medium is associated to the increased concentration of OH^- ions, resulting in increased hydroxylation on the surface of the photocatalyst. This in turn results in a higher concentration of the free radical species ($^{\cdot}OH$), enhancing the overall rate of photodegradation [26].

3.3. Performance of the recycled catalyst

The stability of the silver vanadates and their reusability in the removal of undesirable organic pollutants were studied by examining the photocatalytic degradation using $Ag_4V_2O_7$ for three circulating runs under visible light. The results are illustrated in Fig. 7(a and b) for atrazine and CV, respectively. The photocatalytic activity of $Ag_4V_2O_7$ (Ag3V1-5) was consistent after three successive runs showing 99%, 98%, and 94% degradation of CV, respectively (Fig. 7b). It can be seen from the figure that the XRD patterns of $Ag_4V_2O_7$ powder after the reaction closely match those obtained before reaction although there are some minor differences in the relative intensity of some peaks. It also can be observed that the characteristic peaks of (2 2 0), (0 0 4), (2 2 4), (0 4 0), (0 4 4), and (4 4 4) planes of used catalyst match those peaks of standard XRD JCPDS card for $Ag_4V_2O_7$ [52]. The results clearly show the stability and the insignificant changes in the photocatalyst. $Ag_4V_2O_7$ was also stable for reusing in atrazine degradation, however its performance slightly decreased to 78% after the third run (Fig. 7a). The small decrease in the photocatalytic degradation efficiency might be explained by the unavoidable small loss of the catalyst during each sampling of aliquot for atrazine analysis. Thus, the $Ag_4V_2O_7$ catalyst could be still considered rather stable for reuse. These findings demonstrate the significant stability and practical reusability of silver vanadates in long-term photocatalytic applications without the risk of photocorrosion.

3.4. Photocatalytic reaction mechanism

The role of active species (e.g. holes h^+, hydroxyl radicals ($^{\cdot}OH$), and superoxide radicals ($^{\cdot}O_2^-$)) in the initiation of photocatalytic degradation is well documented [24,25,55–57]. Hence, we set out to

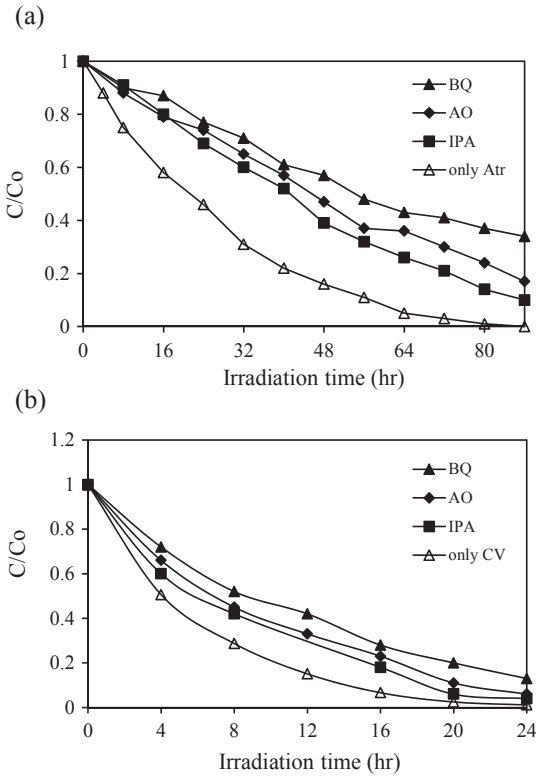

Fig. 8. Photocatalytic degradation of atrazine and CV with silver vanadate catalyst in the absence and presence of scavengers (IPA, AO and BQ) under visible light irradiation. (a) Atrazine ; (b) CV.

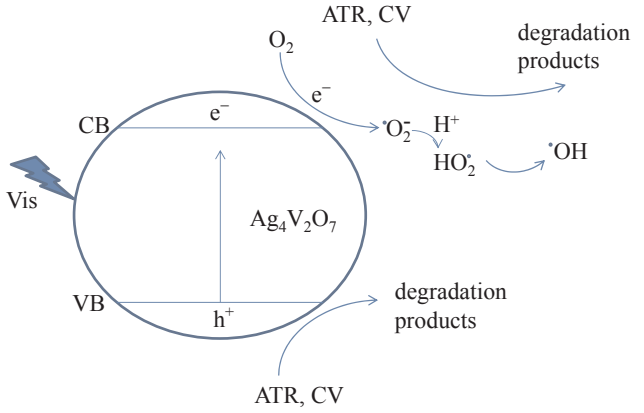

Fig. 9. Schematic diagram illustrating the photocatalytic mechanism of the $Ag_4V_2O_7$ photocatalyst.

investigate the different active species in the photodegradation of atrazine and CV by silver vanadates using three kinds of scavengers. Fig. 8(a and b) displays the results of the degradation of atrazine and CV with $Ag_4V_2O_7$ catalyst under visible light and using different conditions. The photocatalytic degradation of atrazine was 99% after 80 h of treatment in the absence of scavengers. Next, ammonium oxalate (AO) was added as a hole-scavenger [58], reducing the degradation of atrazine to 76%. Therefore, the degradation could be arising, to some extent, from the direct reaction with the photogenerated holes. In addition, the benzoquinone (BQ) significantly suppressed the atrazine degradation to 63% in 80 h of treatment. BQ is known to trap $^{\cdot}O_2^-$ by a simple electron-transfer mechanism [59], which means that $^{\cdot}O_2^-$ might play the most important role in the photocatalytic process. Lastly, the addition of isopropyl alcohol (IPA) as a scavenger for $^{\cdot}OH$,[60] led to a decrease in the atrazine degradation to 86%. These results suggest that $^{\cdot}O_2^-$ radicals are the dominant oxidative species of $Ag_4V_2O_7$, where the $^{\cdot}OH$ and h^+ play an assistant role in the degradation of atrazine. On the other hand, the CV degradations were reduced to a lesser extent upon adding the scavengers [Fig. 8(b)]; with BQ still imposing the strongest effect. The results were thus consistent with those obtained with the photodegradation of atrazine, confirming $^{\cdot}O_2^-$ radicals as the dominant oxidative species.

The photocatalytic mechanism of the $Ag_4V_2O_7$ catalysts can be explained as follows: The irradiation of the $Ag_4V_2O_7$ catalyst with visible light causes excitation of the electrons (e^-) in the valence band (VB) to the conduction band (CB), leaving the same amount of holes (h^+) in the VB. The photogenerated electrons can then reduce O_2 into $^{\cdot}O_2^-$ species, which lastly generate $^{\cdot}OH$ [61]. The active oxygen species or the oxidative holes can attack the pollutants to degrade them gradually. The schematic diagram for the photocatalytic degradation mechanism of CV and atrazine at the surface of $Ag_4V_2O_7$ catalysts under visible light irradiation is illustrated in Fig. 9.

3.5. Separation and identification of the intermediates

Considering the environmental concerns on the atrazine pollutant, we conducted a thorough product study on its degradation in an aqueous solution using the $Ag_4V_2O_7$/visible light process. Fig. 10(a) presents the LC chromatogram of the atrazine solution in the presence of $Ag_4V_2O_7$ catalyst under visible-light irradiation. At least 9 peaks are characterized within a retention time of 50 min in addition to the one attributed to the initial atrazine compound (peak Atr). The intensities of the other nine peaks (1–9) increased firstly and then decreased, signifying that these peaks are the intermediates of the photodegradation, which are subsequently formed and transformed. The molecular assignments of the intermediates of atrazine and their retention times are shown in Table 3. Likewise, Fig. 10(b) displays the LC chromatogram of the CV solution after 12 h of visible-light irradiation. Seven intermediates can be identified in addition to the CV peak that is disappearing slowly. The analysis of the molecular ions peaks and the corresponding fragmentation patterns permitted the structural assignments of the detected intermediates (Table 4).

3.6. Degradation pathways of atrazine and CV dye

The LC/MS identified intermediates led to concluding the possible pathways of the photodegradation of atrazine by silver vanadates. The suggested pathway is depicted in Scheme 1 which is found to be consistent with the atrazine degradation using other photocatalysts [62]. The photodegradation might have proceeded via two types of routes, namely, alkylic–oxidation (parts I and II) and dechlorination–hydroxylation (part III). In the alkylic oxidation process, the hydroxyl radicals can attack either of the ethyl (part I) or isopropyl chains (part II) on the amino groups of the atrazine producing free organic radicals. The oxidations of the radicals yield the intermediates 1 and 2. Further oxidations of the carbon atoms adjacent to the amine functionalities by the hydroxyl radicals followed by dealkylation step generate compounds 4 and 5, and consecutively 7 as intermediates. The second route involves the sequence of dechlorination and hydroxylation of the aromatic position holding the most scissile bond (C-Cl) in the atrazine molecule. This two-step sequence generates the hydroxyatrazine intermediate 3. Then, mono-dealkylation of the alkylamino groups of (3) leads to intermediates 6 and 8. The second dealkylation of these intermediates produces the last compound (9), as identified by our LC-MS analysis. It should be noted that the dechlorination–hydroxylation of intermediate 7 could also produce compound (9).

Regarding the CV degradation pathway (Scheme 2), the N-de-methylation of the CV molecule likely takes place via the attack of the radical species on the N,N-dimethyl group. The dye molecule is adsorbed through the positively-charged dimethylamine functionality,

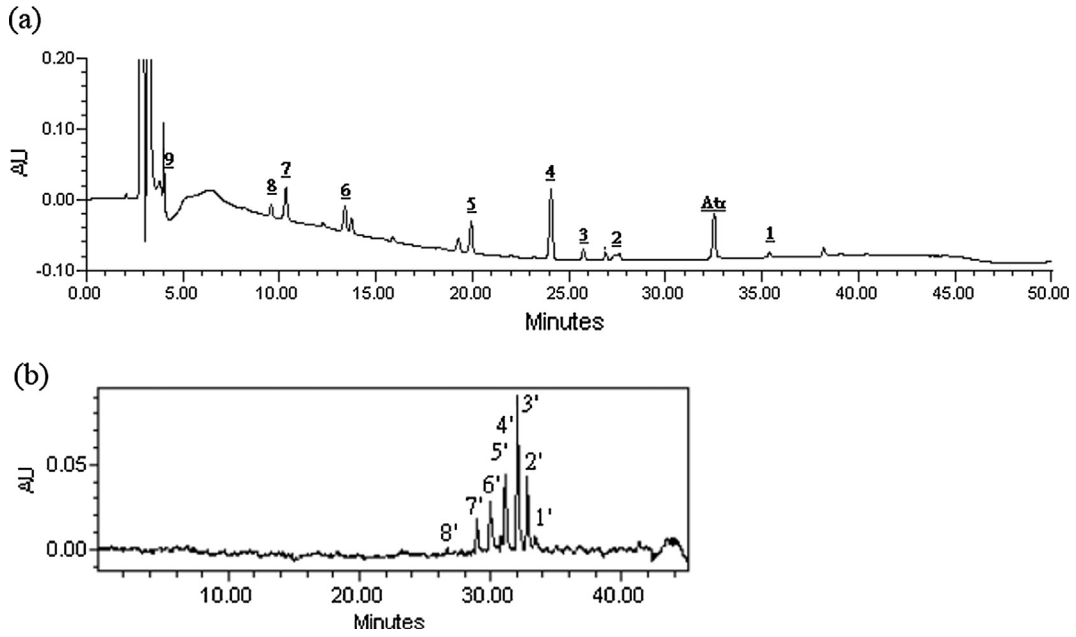

Fig. 10. HPLC chromatogram obtained for (a) atrazine solution (100 mg L^{-1}) after 48 h; (b) CV (100 mg L^{-1}) after 12 h of irradiation with visible light in the presence of silver vanadate catalyst (1.0 g L^{-1}).

Table 3
Identification of the intermediates from the photodegradation of atrazine by LC/MS.

Peaks	Photodegradation intermediates	R.T. (min)	MS peaks (*m/z*)
1	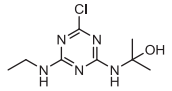	35.48	232
Atr	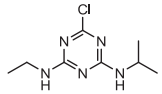	32.61	216
2	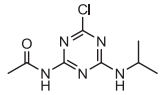	27.35	230
3	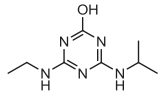	25.90	198
4	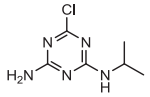	24.17	188
5	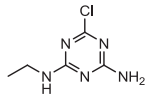	20.11	174
6	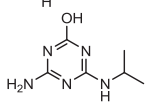	13.51	170
7	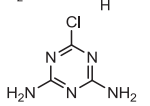	10.44	146
8	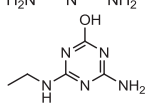	9.76	156
9	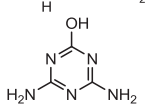	4.09	128

Table 4
Identification of the intermediates from the photodegradation of CV by HPLC-ESI-MS.

Peaks	Photodegradation intermediates	R.T. (min)	MS peaks (*m/z*)
1′	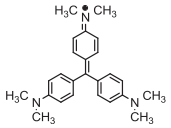	33.37	372
2′	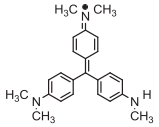	32.77	358
3′	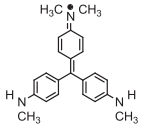	32.04	344
4′	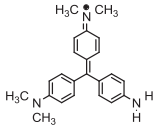	31.12	344
5′	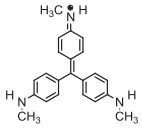	30.77	330
6′	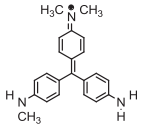	29.97	330
7′	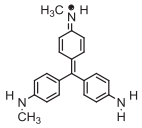	28.96	316
8′	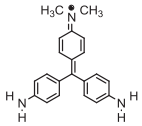	26.72	316

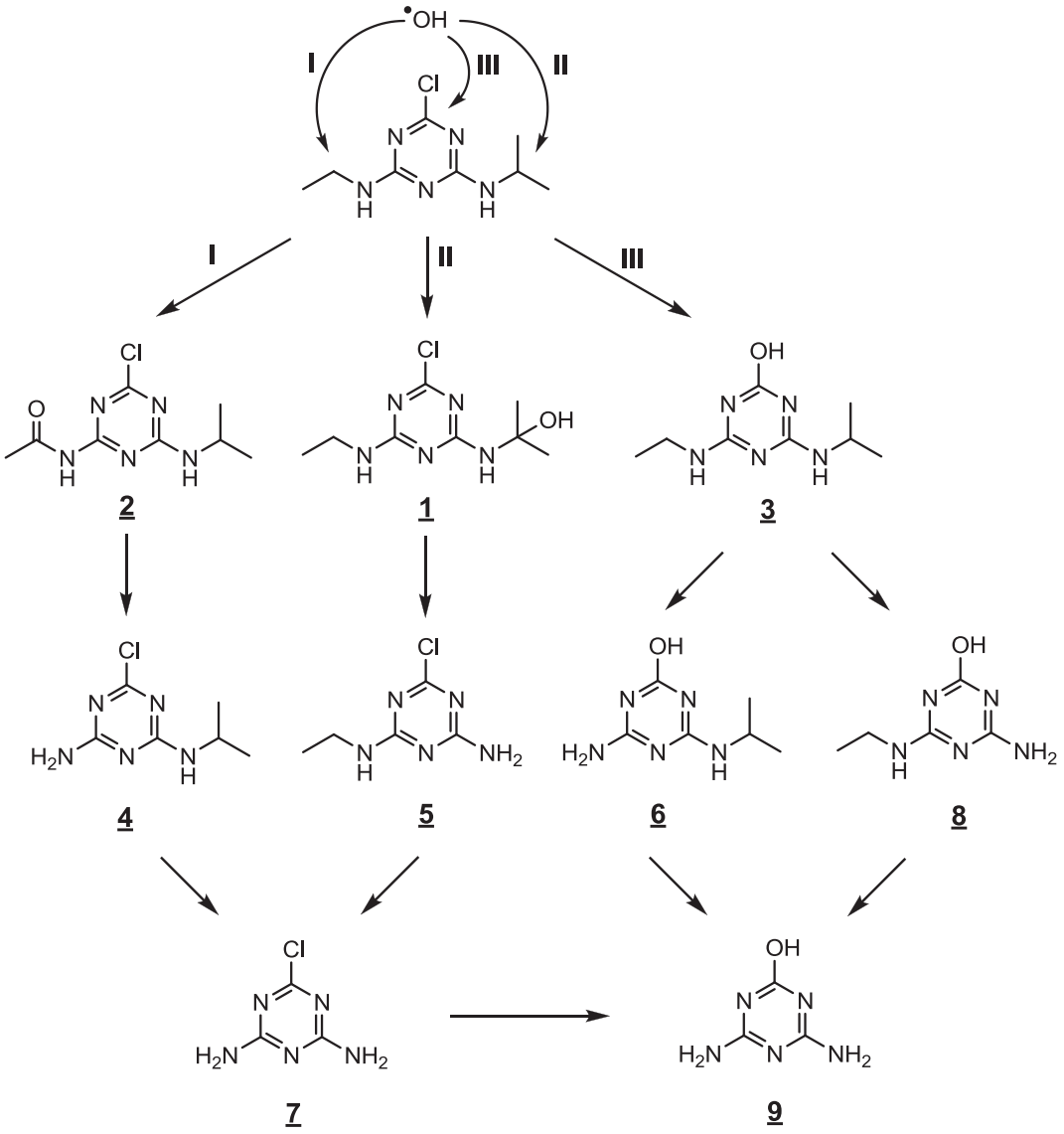

Scheme 1. Proposed photocatalytic degradation pathway of atrazine followed by the identification of several intermediates by HPLC-ESI-MS technique.

which helps in the adsorption of the CV dye on the semiconductor. Two stoichiometric free radicals are involved in a single N-de-methylation. One radical abstracts a hydrogen atom from a methyl substituent of the amino group and another radical attacks on the dimethyl amine leading to mono-demethylation. The positively charged intermediate can also be adsorbed on the photocatalyst surface where stepwise de-methylation of the remaining methylamino groups occurs until producing the completely N-de-methylated adduct. It is worth noting that intermediates that result from the attack of the free radicals on the central carbon of the triphenyl group were less observed in this case, which favors less the other possible degradation pathway by the adsorption of the conjugated dye [63].

4. Conclusion

Silver vanadates have been synthesized by the hydrothermal method. In the current process, the controllable crystal phases and morphologies of the prepared silver vanadates could be achieved by simply changing some hydrothermal parameters such as the molar ratio (Ag/V) and pH value. The materials were characterized by X-ray diffraction (XRD), scanning electron microscopy (SEM), X-ray photoelectron spectroscopy (XPS), and UV–vis diffuse reflectance spectra (DRS). The values of band gaps for all the silver vanadate samples were found to be in the range of 1.85–2.25 eV. The as-prepared silver vanadate catalysts have displayed high photocatalytic activity, which degraded nearly 100% of CV after 24 h under visible-light irradiation and over 97% of atrazine after 72 h of treatment. The high activity can be attributed to their efficient utilization of visible light. The durable photocatalytic activity and chemical stability of the $Ag_4V_2O_7$ catalysts were demonstrated through recycling experiments and the XRD patterns of the catalysts before and after reactions. Moreover, the quenching effects of various scavengers revealed that $^{\cdot}O_2^-$ radicals played a major role while $^{\cdot}OH$ and h^+ played an assistant role in the degradation of atrazine and CV dye. The possible degradation pathways for atrazine were also evaluated exhibiting two different routes: dechlorination–hydroxylation and alkylic-oxidation–de-alkylation. On the other hand, the degradation of the CV dye was proposed to take place via *N*-de-methylation in a stepwise manner producing the various *N*-demethylated intermediate CV species. The excellent activity and photostability reveal that the silver vanadates (including $Ag_4V_2O_7$) are promising visible-light-responsive photocatalysts for water and wastewater treatment.

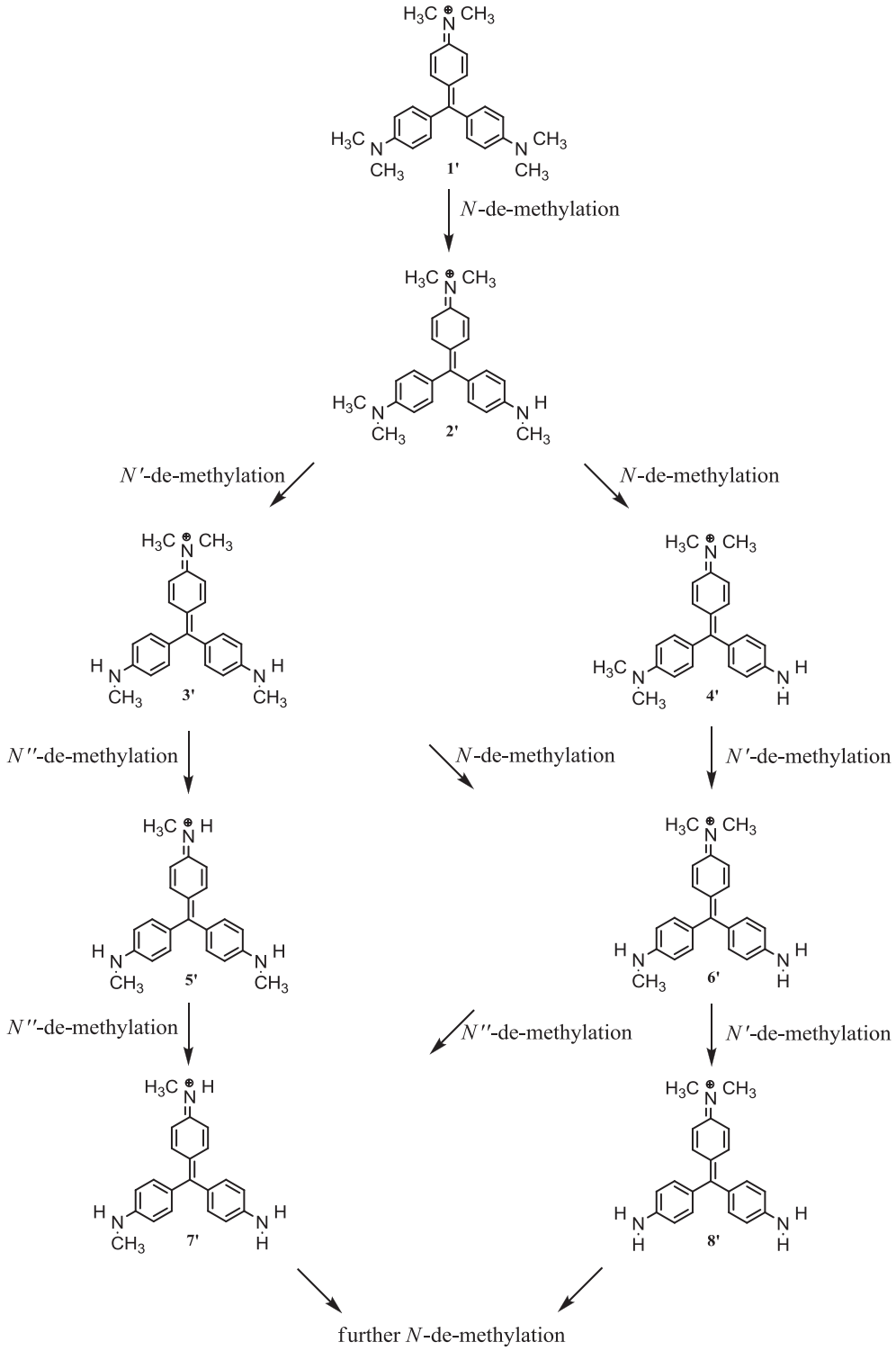

Scheme 2. Proposed photocatalytic degradation pathway of crystal violet followed by the identification of several intermediates by HPLC-ESI-MS technique.

Acknowledgment

This research was supported by the Ministry of Science and Technology of the Republic of China (MOST 105-2113-M-025-001).

Appendix A. Supplementary material

Supplementary data associated with this article can be found, in the online version, at https://doi.org/10.1016/j.seppur.2018.06.011.

References

[1] C.-M. Huang, G.-T. Pan, Y.-C.M. Li, M.-H. Li, T.C.K. Yang, Crystalline phases and photocatalytic activities of hydrothermal synthesis Ag_3VO_4 and $Ag_4V_2O_7$ under visible light irradiation, Appl. Catal. A-Gen. 358 (2009) 164–172.
[2] C. Belver, M. Hinojosa, J. Bedia, M. Tobajas, M. Alvarez, V. Rodríguez-González, J.J. Rodriguez, Ag-coated heterostructures of ZnO-TiO_2/delaminated montmorillonite as solar photocatalysts, Materials 10 (2017) 960.
[3] H. Shi, Z. Li, J. Kou, J. Ye, Z. Zou, Facile synthesis of single-crystalline $Ag_2V_4O_{11}$ nanotube material as a novel visible-light-sensitive photocatalyst, J. Phys. Chem. C 115 (2011) 145–151.

[4] X. Lin, Y. Xi, R. Zhao, J. Shi, N. Yan, Construction of C_{60}-decorated SWCNTs (C_{60}-CNTs)/bismuth-based oxide ternary heterostructures with enhanced photocatalytic activity, RSC Adv. 7 (2017) 53847–53854.

[5] X. Lin, D. Xu, S. Jiang, F. Xie, M. Song, H. Zhai, L. Zhao, G. Che, L. Chang, Graphitic carbon nitride nanocrystals decorated $AgVO_3$ nanowires with enhanced visible-light photocatalytic activity, Catal. Commun. 89 (2017) 96–99.

[6] X. Lin, D. Xu, R. Zhao, Y. Xi, L. Zhao, M. Song, H. Zhai, G. Che, L. Chang, Highly efficient photocatalytic activity of g-C_3N_4 quantum dots (CNQDs)/Ag/Bi_2MoO_6 nanoheterostructure under visible light, Sep. Purif. Technol. 178 (2017) 163–168.

[7] X. Lin, D. Xu, Y. Xi, R. Zhao, L. Zhao, M. Song, H. Zhai, G. Che, L. Chang, Construction of leaf-like g-C_3N_4/Ag/$BiVO_4$ nanoheterostructures with enhanced photocatalysis performance under visible-light irradiation, Colloid Surf. A-Physicochem. Eng. Asp. 513 (2017) 117–124.

[8] R. Ran, X. Meng, Z. Zhang, Facile preparation of novel graphene oxide-modified Ag_2O/Ag_3VO_4/$AgVO_3$ composites with high photocatalytic activities under visible light irradiation, Appl. Catal. B-Environ. 196 (2016) 1–15.

[9] S. Jonjana, A. Phuruangrat, S. Thongtem, O. Wiranwetchayan, T. Thongtem, Preparation and characterization of Ag_3VO_4/Bi_2MoO_6 nanocomposites with highly visible-light-induced photocatalytic properties, Mater. Lett. 180 (2016) 93–96.

[10] F. Wang, H. Zhang, L. Liu, B. Shin, F. Shan, AgV_7O_{18}: A new silver vanadate semiconductor with photodegradation ability on dyes under visible-light irradiation, Mater. Lett. 169 (2016) 82–85.

[11] C.-M. Huang, K.-W. Cheng, G.-T. Pan, W.-S. Chang, T.C.K. Yang, CTAB-assisted hydrothermal synthesis of silver vanadates and their photocatalytic characterization, Chem. Eng. Sci. 65 (2010) 148–152.

[12] L. Liang, Y. Xu, Y. Lei, H. Liu, 1-Dimensional $AgVO_3$ nanowires hybrid with 2-dimensional graphene nanosheets to create 3-dimensional composite aerogels and their improved electrochemical properties, Nanoscale 6 (2014) 3536–3539.

[13] M.R. Parida, C. Vijayan, C.S. Rout, C.S. Suchand Sandeep, R. Philip, Enhanced optical nonlinearity in β-$AgVO_3$ nanobelts on decoration with Ag nanoparticles, Appl. Phys. Lett. 100 (2012) 121119.

[14] R. Konta, H. Kato, H. Kobayashi, A. Kudo, Photophysical properties and photocatalytic activities under visible light irradiation of silver vanadates, Phys. Chem. Chem. Phys. 5 (2003) 3061–3065.

[15] Y. Sang, L. Kuai, C. Chen, Z. Fang, B. Geng, Fabrication of a visible-light-driven plasmonic photocatalyst of $AgVO_3$@AgBr@Ag nanobelt heterostructures, ACS Appl. Mater. Interfaces 6 (2014) 5061–5068.

[16] S. Nagamuthu, S. Vijayakumar, K.-S. Ryu, Synthesis of Ag anchored Ag_3VO_4 stacked nanosheets: toward a negative electrode material for high-performance asymmetric supercapacitor devices, J. Phys. Chem. C 120 (2016) 18963–18970.

[17] R.C. de Oliveira, M. Assis, M.M. Teixeira, M.D.P. da Silva, M.S. Li, J. Andres, L. Gracia, E. Longo, An experimental and computational study of β-$AgVO_3$: Optical properties and formation of Ag nanoparticles, J. Phys. Chem. C 120 (2016) 12254–12264.

[18] D. McNulty, Q. Ramasse, C. O'Dwyer, The structural conversion from α-$AgVO_3$ to β-$AgVO_3$: Ag nanoparticle decorated nanowires with application as cathode materials for Li-ion batteries, Nanoscale 8 (2016) 16266–16275.

[19] J.-M. Song, Y.-Z. Lin, H.-B. Yao, F.-J. Fan, X.-G. Li, S.-H. Yu, Superlong β-$AgVO_3$ nanoribbons: High-yield synthesis by a pyridine-assisted solution approach, their stability, electrical and electrochemical properties, ACS Nano 3 (2009) 653–660.

[20] J. Wang, H. Ruan, W. Li, D. Li, Y. Hu, J. Chen, Y. Shao, Y. Zheng, Highly efficient oxidation of gaseous benzene on novel Ag_3VO_4/TiO_2 nanocomposite photocatalysts under visible and simulated solar light irradiation, J. Phys. Chem. C 116 (2012) 13935–13943.

[21] E. Akbarzadeh, S.R. Setayesh, M.R. Gholami, Synthesis of the visible-light-driven Ag_3VO_4/Ag_3PO_4/Ag photocatalysts with enhanced photocatalytic activity, RSC Adv. 6 (2016) 14909–14915.

[22] J. Wang, X. Yang, J. Chen, J. Xian, S. Meng, Y. Zheng, Y. Shao, D. Li, Photocatalytic activity of novel $Ag_4V_2O_7$ photocatalyst under visible light irradiation, J. Am. Ceram. Soc. 97 (2013) 267–274.

[23] Y. Xue, X. Wang, The effects of Ag doping on crystalline structure and photocatalytic properties of $BiVO_4$, Int. J. Hydrog. Energy 40 (2015) 5878–5888.

[24] S. Huang, C. Chen, H. Tsai, J. Shaya, C. Lu, Photocatalytic degradation of thiobencarb by a visible light-driven MoS_2 photocatalyst, Sep. Purif. Technol. 197 (2018) 147–155.

[25] Y. Wu, C. Chen, Y. Huang, W. Lin, Y. Yen, C. Lu, Pirimicarb degradation by $BiVO_4$ photocatalysis: Parameter and reaction pathway investigations, Sep. Sci. Technol. 51 (2016) 2284–2296.

[26] R.-J. Wu, C.-C. Chen, C.-S. Lu, P.-Y. Hsu, M.-H. Chen, Phorate degradation by TiO_2 photocatalysis: Parameter and reaction pathway investigations, Desalination 250 (2010) 869–875.

[27] H.-F. Lai, C.-C. Chen, R.-J. Wu, C.-S. Lu, Thiobencarb degradation by TiO_2 photocatalysis: Parameter and reaction pathway investigations, J. Chin. Chem. Soc. 59 (2012) 87–97.

[28] C.-C. Chen, R.-J. Wu, Y.-Y. Tzeng, C.-S. Lu, Chemical oxidative degradation of acridine orange dye in aqueous solution by Fenton's reagent, J. Chin. Chem. Soc. 56 (2009) 1147–1155.

[29] K. Kerminen, M.H. Kontro, Sonication effects on atrazine dissipation in vadose zone sediment slurries, Environments 4 (2017) 18.

[30] H. Prosen, M. Gucek, L. Zupancic-Kralj, Optimization of liquid chromatography and micellar electrokinetic chromatography for the determination of atrazine and its first degradation products in humic waters without sample preparation, Chromatographia 60 (2004) S107–S112.

[31] X.-Y. Song, J.-N. Li, Y.-P. Wu, B. Zhang, B.-X. Li, Atrazine causes autophagy- and apoptosis-related neurodegenerative effects in dopaminergic neurons in the rat nigrostriatal dopaminergic system, Int. J. Mol. Sci. 16 (2015) 13490–13506.

[32] US EPA - Pesticides - Triazine cumulative risk assessment, (2006) 1–67.

[33] F.M. Drumond Chequer, G.A.R. de Oliveira, E.R. Anastacio Ferraz, J. Carvalho, M.V. Boldrin Zanoni, D.P. de Oliveir, Textile dyes: Dyeing process and environmental impact, Eco-friendly textile dyeing and finishing, In Tech, 2013, pp. 1–26, , http://dx.doi.org/10.5772/53659.

[34] R.M. El-Shishtawy, Functional dyes, and some Hi-Tech applications, Int. J. Photoenergy (2009) 1–21, http://dx.doi.org/10.1155/2009/434897.

[35] J. Shaya, M. Collot, F. Bénailly, N. Mahmoud, Y. Mély, B.Y. Michel, A.S. Klymchenko, A. Burger, Turn-on fluorene push–pull probes with high brightness and photostability for visualizing lipid order in biomembranes, ACS Chem. Biol. 12 (2017) 3022–3030.

[36] J. Shaya, F. Fontaine-Vive, B.Y. Michel, A. Burger, Rational design of push-pull fluorene dyes: synthesis and structure-photophysics relationship, Chem. Eur. J. 22 (2016) 10627–10637.

[37] N.P.F. Barthes, K. Gavvala, D. Dziuba, D. Bonhomme, I.A. Karpenko, A.S. Dabert-Gay, D. Debayle, A.P. Demchenko, R. Benhida, B.Y. Michel, Y. Mély, A. Burger, Dual emissive analogue of deoxyuridine as a sensitive hydration-reporting probe for discriminating mismatched from matched DNA from DNA/DNA and DNA/RNA duplexes, J. Mater. Chem. C 4 (2016) 3010–3017.

[38] J. Shaya, M.-A. Deschamps, B.Y. Michel, A. Burger, Air-stable Pd catalytic systems for sequential one-pot synthesis of challenging unsymmetrical aminoaromatics, J. Org. Chem. 81 (2016) 7566–7573.

[39] S. Mani, R.N. Bharagava, Exposure to crystal violet, its toxic, genotoxic and carcinogenic effects on environment and its degradation and detoxification for environmental safety, Rev. Environ. Contam. Toxicol. 237 (2016) 71–104.

[40] M. Doğan, H. Abak, M. Alkan, Adsorption of methylene blue onto hazelnut shell: Kinetics, mechanism and activation parameters, J. Hazard. Mater. 164 (2009) 172–181.

[41] C. Lu, Y. Wu, F. Mai, W. Chung, C. Wu, W. Lin, C. Chen, Degradation efficiencies and mechanisms of the ZnO-mediated photocatalytic degradation of Basic Blue 11 under visible light irradiation, J. Mol. Catal. A-Chem. 310 (2009) 159–165.

[42] C.-S. Lu, F.-D. Mai, C.-W. Wu, R.-J. Wu, C.-C. Chen, Titanium dioxide-mediated photocatalytic degradation of Acridine Orange in aqueous suspensions under UV irradiation, Dyes Pigment. 76 (2008) 706–713.

[43] C.-C. Chen, H.-J. Fan, C.-Y. Jang, J.-L. Jan, H.-D. Lin, C.-S. Lu, Photooxidative N-demethylation of crystal violet dye in aqueous nano-TiO_2 dispersions under visible light irradiation, J. Photochem. Photobiol. A-Chem. 184 (2006) 147–154.

[44] Y. Lu, Y. Wan, S. Bi, H. Weng, Y. Huang, L. Qin, H.J. Seo, Synthesis, surface and optical properties of $Ag_2CaV_4O_{12}$ nanoparticles for dye removal under visible irradiation, Mater. Chem. Phys. 180 (2016) 263–271.

[45] A. Habibi-Yangjeh, M. Shekofteh-Gohari, Fe_3O_4/ZnO/Ag_3VO_4/AgI nanocomposites: Quaternary magnetic photocatalysts with excellent activity in degradation of water pollutants under visible light, Sep. Purif. Technol. 166 (2016) 63–72.

[46] H.-F. Lai, C.-C. Chen, Y.-K. Chang, C.-S. Lu, R.-J. Wu, Efficient photocatalytic degradation of thiobencarb over $BiVO_4$ driven by visible light: Parameter and reaction pathway investigations, Sep. Purif. Technol. 122 (2014) 78–86.

[47] C.-C. Chen, C.-S. Lu, F.-D. Mai, C.-S. Weng, Photooxidative N-de-ethylation of anionic triarylmethane dye (sulfan blue) in titanium dioxide dispersions under UV irradiation, J. Hazard. Mater. 137 (2006) 1600–1607.

[48] L.-C. Chen, G.-T. Pan, T.C.K. Yang, T.-W. Chung, C.-M. Huang, In situ DRIFT and kinetic studies of photocatalytic degradation on benzene vapor with visible-light-driven silver vanadates, J. Hazard. Mater. 178 (2010) 644–651.

[49] M. Shang, W. Wang, L. Zhou, S. Sun, W. Yin, Nanosized $BiVO_4$ with high visible-light-induced photocatalytic activity: Ultrasonic-assisted synthesis and protective effect of surfactant, J. Hazard. Mater. 172 (2009) 338–344.

[50] M.A. Butler, Photoelectrolysis and physical properties of the semiconducting electrode WO_3, J. Appl. Phys. 48 (1977) 1914–1920.

[51] W.W. Lee, C.-S. Lu, C.-W. Chuang, Y.-J. Chen, J.-Y. Fu, C.-W. Siao, C.-C. Chen, Synthesis of bismuth oxyiodides and their composites: characterization, photocatalytic activity, and degradation mechanisms, RSC Adv. 5 (2015) 23450–23463.

[52] R. Ran, J.G. McEvoy, Z. Zhang, Ag_2O/Ag_3VO_4/$Ag_4V_2O_7$ heterogeneous photocatalyst prepared by a facile hydrothermal synthesis with enhanced photocatalytic performance under visible light irradiation, Mater. Res. Bull. 74 (2016) 140–150.

[53] D.W. Hwang, K.Y. Cha, J. Kim, H.G. Kim, S.W. Bae, J.S. Lee, Photocatalytic degradation of CH_3Cl over a nickel-loaded layered perovskite, Ind. Eng. Chem. Res. 42 (2003) 1184–1189.

[54] X. Zhu, C. Yuan, Y. Bao, J. Yang, Y. Wu, Photocatalytic degradation of pesticide pyridaben on TiO_2 particles, J. Mol. Catal. A-Chem. 229 (2005) 95–105.

[55] C.-S. Lu, C.-C. Chen, L.-K. Huang, P.-A. Tsai, H.-F. Lai, Photocatalytic degradation of acridine orange over $NaBiO_3$ driven by visible light irradiation, Catalysts 3 (2013) 501–516.

[56] C.-C. Chen, R.-J. Wu, I.C. Yao, C.-S. Lu, Bis(2-chloroethoxy)methane degradation by TiO_2 photocatalysis: Parameter and reaction pathway investigations, J. Hazard. Mater. 172 (2009) 1021–1032.

[57] R.-J. Wu, C.-C. Chen, M.-H. Chen, C.-S. Lu, Titanium dioxide-mediated heterogeneous photocatalytic degradation of terbufos: Parameter study and reaction pathways, J. Hazard. Mater. 162 (2009) 945–953.

[58] H. Kominami, A. Furusho, S.-Y. Murakami, H. Inoue, Y. Kera, B. Ohtani, Effective

photocatalytic reduction of nitrate to ammonia in an aqueous suspension of metal-loaded titanium(IV) oxide particles in the presence of oxalic acid, Catal. Lett. 76 (2001) 31–34.
[59] M. Stylidi, Visible light-induced photocatalytic degradation of Acid Orange 7 in aqueous TiO_2 suspensions, Appl. Catal. B-Environ. 47 (2004) 189–201.
[60] K. Lv, Y. Xu, Effects of polyoxometalate and fluoride on adsorption and photocatalytic degradation of organic dye X3B on TiO_2: The difference in the production of reactive species, J. Phys. Chem. B 110 (2006) 6204–6212.
[61] P. Ju, H. Fan, S. Ai, D. Zhang, Y. Wang, Photocatalytic activity of one-dimensional $Ag_2V_4O_{11}$ nanowires in the degradation of bisphenol A under visible-light irradiation, Res. Chem. Intermed. 41 (2015) 3683–3697.
[62] L. Xu, H. Zang, Q. Zhang, Y. Chen, Y. Wei, J. Yan, et al., Photocatalytic degradation of atrazine by $H_3PW_{12}O_{40}$/Ag-TiO_2: kinetics, mechanism and degradation pathways, Chem. Eng. J. 232 (2013) 174–182.
[63] H.-J. Fan, S.-T. Huang, W.-H. Chung, J.-L. Jan, W.-Y. Lin, C.-C. Chen, Degradation pathways of crystal violet by Fenton and Fenton-like systems: Condition optimization and intermediate separation and identification, J. Hazard. Mater. 171 (2009) 1032–1044.